A Versatile Setup for Determining Hydrogen and Oxygen Crossover of Electrolyzer Membranes and MEAs

Leander Treutlein*, Ali Javed, Tobias Hilche, Hans Kungl, André Karl, Eva Jodat and Rüdiger-A. Eichel

DOI: 10.1002/cite.70031

Hydrogen and oxygen crossover in polymer electrolyte membrane (PEM) electrolyzers is critical for both operational safety and product gas purity. In this study, we present a versatile experimental setup designed to quantify gas crossover through membranes and polymers commonly used in PEM electrolyzers. A key feature of the setup is its ability to perform in situ measurements on fully assembled PEM cells, containing complete membrane electrode assemblies. The system also enables characterization of gas permeation through both wet and dry ionomers, as well as various polymers employed in components such as gaskets and tubing. These capabilities are demonstrated through a series of representative measurements that highlight the setup's flexibility and potential.

Keywords: Gas crossover, Gas crossover setup, Gas sensor, Hydrogen, Ionomer, Nafion, PEM electrolysis, Pinholes

Received: May 27, 2025; *revised:* August 28, 2025; *accepted:* September 10, 2025

1 Introduction

To address climate change and facilitate the transition to a sustainable energy economy, the production of green hydrogen from renewable energy sources has emerged as a key enabling technology for both research and industrial applications. Water electrolyzers play a central role in this context, converting electricity generated from renewable sources into green hydrogen. However, scaling up electrolyzer systems for commercial deployment requires the implementation of de-risking strategies to gain insights into degradation mechanisms by identifying the key factors contributing to performance or efficiency loss [1]. One notable degradation effect is the increase of gas crossover, an effect in which hydrogen or oxygen permeates through the membrane that separates the anodic and cathodic compartments. This phenomenon is closely linked to both operational conditions and the intrinsic properties of the membrane materials. The hydrogen and oxygen crossover is mainly influenced by variables such as operating pressure [2], current density [3], cell temperature [4], cell assembly [5, 6], and (membrane) material [7]. A higher quantity of gas crossover can significantly reduce gas purity [8], decrease total system efficiency [8], pose safety issues [9], and increase the rate of cell degradation [10]. Although crossover is relevant to all water–electrolyzer technologies, this study focuses on proton exchange membrane electrolysis cells (PEMECs). In PEMECs, crossover-driven degradation can become self-amplifying: Hydrogen or oxygen that permeates the membrane can form hydrogen peroxide (H_2O_2) at catalytic sites [11], and H_2O_2 can form reactive radicals that chemically attack the polymer membrane [12]. This chemical attack causes thinning, microcracking, or pinhole formation [7], which in turn increases gas crossover and further accelerates degradation and the associated losses in purity, efficiency, and safety.

Considering the materials' characteristics and the impact of operational parameters on the performance and service life, it is essential to choose suitable materials, especially for the membrane, during the design phase of an electrolyzer. In this context, gas permeability and proton conductivity

[1,2]Leander Treutlein https://orcid.org/0009-0001-8989-5239 (l.treutlein@fz-juelich.de), [1]Dr. Ali Javed https://orcid.org/0000-0002-9947-0904, [1]Dr. Tobias Hilche https://orcid.org/0009-0000-6603-1377, [1]Dr. Hans Kungl https://orcid.org/0000-0003-3142-3906, [1]Dr. André Karl https://orcid.org/0000-0003-2289-5987, [1]Dr. Eva Jodat https://orcid.org/0009-0004-8214-2981, [1,2,3]Prof. Rüdiger-A. Eichel https://orcid.org/0000-0002-0013-6325

[1]Institute of Energy Technologies, Fundamental Electrochemistry (IET-1), Forschungszentrum Jülich, 52425 Jülich, Germany.

[2]Institute of Physical Chemistry, RWTH Aachen University, 52074 Aachen, Germany.

[3]Faculty of Mechanical Engineering, RWTH Aachen University, 52062 Aachen, Germany.

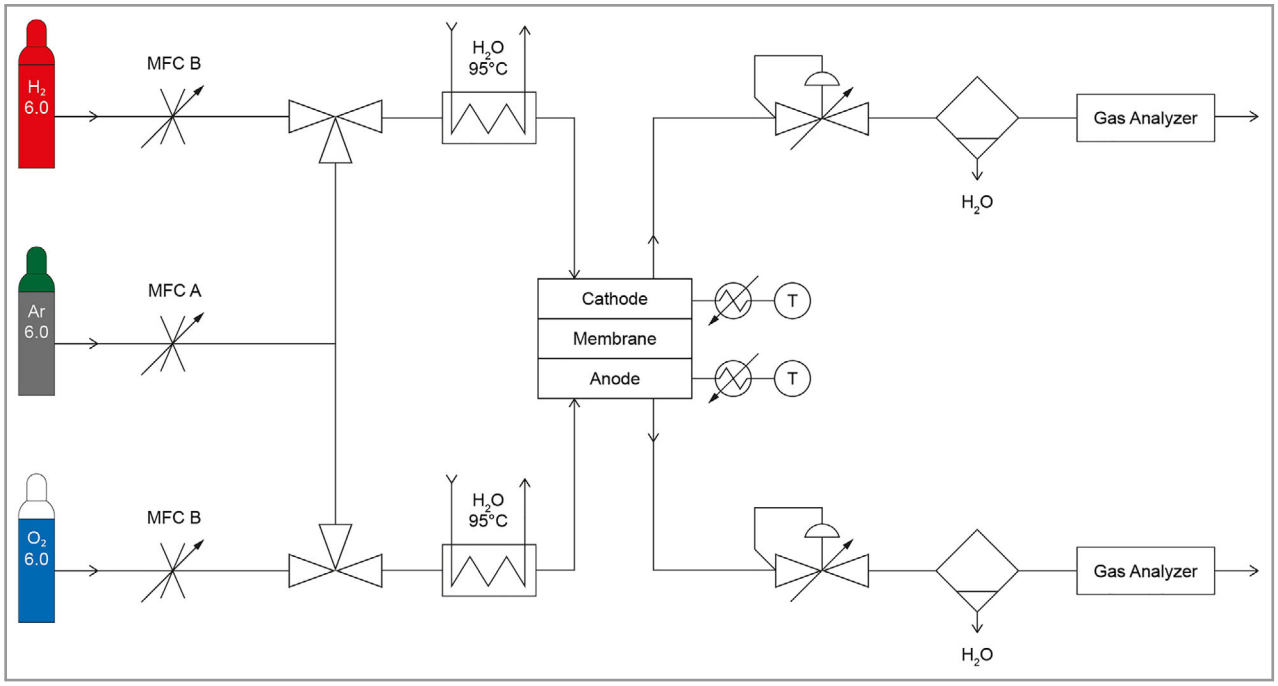

Figure 1. Layout of the gas crossover setup, with the gas flowing from left to right. On the left most side is the gas supply with mass flow controllers (MFC), then gas humidification, measurement cell, pressure control, dehumidification, and lastly gas analysis.

are crucial intrinsic properties, and the optimal membrane material should allow high proton conductivity while minimizing the gas crossover in real-world settings [13]. The gas crossover can be reduced by increasing the membrane thickness; however, it simultaneously increases the total ohmic resistance of the cell, demonstrating a significant challenge [14]. Therefore, to evaluate the performance of a membrane, it is essential to assess the gas crossover and proton ohmic resistance prior to electrolysis operation [15]. But as important as choosing a fitting membrane before assembly of the PEMEC is how catalyst coating of the membrane and operation parameters (including beginning-of-operation) affect long-term ohmic resistance and gas crossover of the membrane electrode assembly (MEA). Inside a cell assembly the ohmic resistance of the membrane is usually assessed using impedance spectroscopy [16]. But, for gas crossover assessment, the most used technique is H_2 in O_2 and O_2 in H_2 measurement during electrolysis via gas analysis [17–21]; this comes with two important downsides: (i) Oxygen crossover can be falsified due to recombination with hydrogen [22] and (ii) hydrogen crossover can be influenced by water drag through the membrane and supersaturation in the catalyst layer [23]. Other techniques rely on purpose-built cell designs [4, 24–26], where the effects of electrolyzer operation cannot be investigated without first disassembling the PEMEC and putting it into the measurement cell. This process is both time-consuming and may affect the characteristics of the membrane via handling.

In addition to bulk transport phenomena, localized defects such as pinholes in the membrane must be identified after the assembly of the PEMEC, as they significantly increase the risk of gas crossover. Moreover, gas permeation through other cell components, such as gaskets and tubing, can result in minor losses of the produced gases to the environment. To comprehensively assess these factors, a holistic approach is required to evaluate the hydrogen and oxygen permeability of all materials used in a polymer electrolyte membrane (PEM) electrolyzer. This study presents a non-electrochemical setup capable of detecting hydrogen and oxygen crossover under both dry and humidified conditions. The system is versatile and can be applied to characterize membranes, MEAs, or other cell components. Importantly, it enables the in situ characterization of MEA gas permeability in a fully assembled PEMEC in parallel to long-term operation, requiring only brief interruptions to the experiment for crossover assessment.

2 Experimental Procedures

2.1 Setup

Fig. 1 illustrates the P&ID diagram of the gas-sensing setup developed to measure gas crossover. The gases flowing into the system were regulated by mass flow controllers (argon: Bronkhorst F-201CV, oxygen and hydrogen: Sensirion

SFC5500). Afterward, the cathode side of the cell can be either flushed by argon or hydrogen, and the anode side can be either flushed with argon or oxygen. In the following text, the side where argon is flushed will be called measurement side, whereas the oxygen or hydrogen side will be called permeate side. The gas supplied to the cell was humidified by membrane humidifiers (Permapure MH-110-42), and the dew point of the gases was regulated by the water temperature flowing through the humidifier. In this regard, the cell was kept fully humidified by ensuring slight condensation consistently occurred inside the cell. This was achieved by setting up the humidifier's temperature 5 K above cell temperature.

In this way, MEAs were prevented from drying out, and the measurements were conducted under fully humidified conditions. For measurements of dry membranes, the humidifier was removed from the system. Back pressure regulators (Equilibar ZF-Series) were used to set the pressure of the permeate gas inside the cell. Before measuring the concentration of permeate (in this work, hydrogen or oxygen as a permeate) in the carrier gas, gases were dried by a gas cooler (M&C Techgroup ECP2000) to achieve consistent humidity levels inside the gas analyzer. Then, detectors monitored the concentration of hydrogen or oxygen in argon via change in thermal conductivity (Messkonzept FTC320). This measurement method is especially fitting for this task, as these can measure gas concentration continuously. A gas chromatograph, for example, would only take a sample of the gas every few minutes.

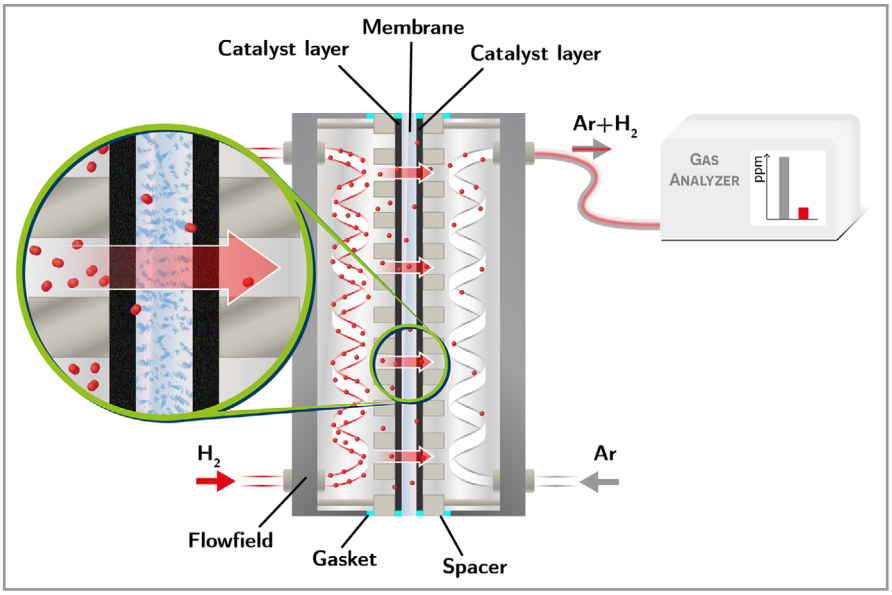

Figure 2. Illustration of the apparatus used to measure hydrogen or oxygen gas crossover. Red bubbles illustrate hydrogen molecules in the system. The red arrow indicates the direction of diffusion through the membrane. The gray gas stream is the argon carrier gas stream.

The following steps outline the approach that was used to measure the pressure-dependent gas permeation using the setup shown in Fig. 1:

1. Anode and cathode were flushed with (humidified) argon for 2 h until gas analyzers indicated stable readings.
2. The gas flows at anode and cathode were adjusted to 70 nmL min^{-1} (mL at normal conditions), and gas analyzers were calibrated to zero-point.
3. (Humidified) hydrogen at cathode side (or [humidified] oxygen at anode side for oxygen crossover) was flushed for 30 min with flow rate 200 nmL min^{-1}. The cathode pressure (anode pressure for oxygen crossover) was raised to 5 bara (5 bar of absolute pressure) and again purged for 30 min.
4. The cell temperature was set to 60 °C, and pressure on the anode and cathode side was set to ambient. After 15 min the first permeability measurement at ambient pressure was taken.
5. The pressure of the measurement gas (hydrogen or oxygen) is stepwise increased from 1 to 5 bara in 500 mbar steps; at each step after 15 min, a measurement is taken.
6. This pressure cycle (1–5 bara) was repeated three times to ensure sample stability.

Alternatively, temperature-dependent permeability can also be measured. Here the steps are like the beforehand outlined approach. Instead of changing pressure, the temperature of the cell with the sample was varied (40–80 °C, in 5 K steps), and the pressure was kept constant at 4 bara.

2.2 Evaluation

Fig. 2 illustrates the operating principle of the setup developed in this study for hydrogen crossover measurements. In the electrolysis cell, one compartment was purged with the measurement gas (hydrogen 6.0 or oxygen 6.0), whereas the opposite side was flushed with argon 6.0 as a carrier gas at a known volumetric flow rate $\dot{V}_{Ar,n}$.

Calibration of the thermal conductivity detector was performed after commissioning the setup by directly mixing hydrogen into the argon stream. The resulting calibration curve, shown in Fig. 3a, demonstrates good linearity up to 5 vol %. Beyond this concentration, deviations appear, as expected, because the sensor is factory-calibrated only in the 0–5 vol % range. To ensure accuracy, all measurements were conducted below 5 vol % hydrogen by adjusting the argon flow rate for each sample accordingly.

The measurement gas diffuses through the membrane into the carrier gas stream. Thereafter, the concentration of

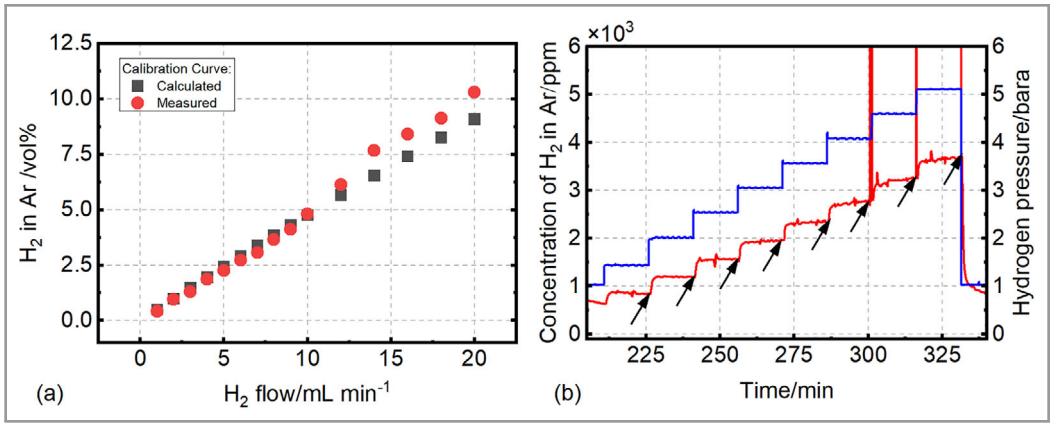

Figure 3. (a) Calibration curve of the TCD for argon in hydrogen. The device is calibrated for a range of 0–5 vol %. (b) Concentration of hydrogen in argon for an unconditioned N117-based MEA. Color scheme: red line: hydrogen concentration, blue line: cell pressure. Black arrows indicate the values used to calculate the permeation. The spikes in the permeate value originate from periodic water dispersal of the gas dryer.

hydrogen in argon ($X_{H_2/Ar}$) was measured. Fig. 3b shows this concentration value for a measurement, where the pressure is varied as an example. At each instance marked with a black arrow, a 60 s interval of the measurement was taken and the mean value used for the evaluation. Based on the measured value of $R_{H_2/Ar}$, the flow rate of hydrogen through the membrane can be calculated:

$$\dot{V}_{H_2} = \frac{X_{H_2/Ar} \cdot \dot{V}_{Ar,ac}}{1 - X_{H_2/Ar}} \tag{1}$$

Flow rate of argon as a carrier gas was measured at normal conditions (273.15 K and 1.01325 bara), which was corrected to flow rate $\dot{V}_{Ar,ac}$ at actual conditions inside the gas analyzer. Here, the temperature of the sensor T_{ac} (336.15 K) and the internal pressure P_{ac} were used. This was achieved using the combined gas law:

$$\dot{V}_{Ar,ac} = \dot{V}_{Ar,n} \cdot \frac{T_{ac}}{T_n} \cdot \frac{P_n}{P_{ac}} \tag{2}$$

This volumetric flow was transferred into a molar flow to perform a comparison at different temperatures. So, the ideal gas law with the gas constant R was used:

$$\dot{n}_{H_2} = \frac{P_{ac} \cdot \dot{V}_{H_2}}{R \cdot T_{ac}} \tag{3}$$

The molar flow rate shown in Eq. (3) represents the crossover rate of the gas through the membrane, which allows a comparison independent of sample size and thickness. For comparison of different sample sizes, the permeation e_{H_2} in the following equation is used, where the crossover rate is normalized to the cell area A:

$$e_{H_2} = \frac{\dot{n}_{H_2}}{A} \tag{4}$$

Eq. (5) represents the intrinsic property of permeability ε_{H_2}. Here, the value is normalized with the thickness L of the sample and the partial pressure of hydrogen p_{H_2}:

$$\varepsilon_{H_2} = \frac{L \cdot e_{H_2}}{p_{H_2}} \tag{5}$$

For a fully humidified cell, the total pressure of the measurement gas side is equal to the combined value of the partial pressure of supplied gas and the partial pressure of water [4]. Hence, the hydrogen partial pressure needs to be adjusted by subtracting the water vapor pressure p_{H_2O} at the cell temperature T_{cell}. The water vapor pressure is calculated using the Antoine equation [27]:

$$p_{H_2O} = \frac{10^{8.07131 - (1730.36\ \mathrm{K}/(233.426\ \mathrm{K} + T_{cell}))}}{747.769} \tag{6}$$

$$p_{H_2,ac} = p_{H_2} - p_{H_2O} \tag{7}$$

2.3 Sample Preparation

The samples investigated in this work are divided into three groups, depending on which they were prepared accordingly. The PEM membranes and MEAs (Nafion N117, N115) were placed in deionized water at 80 °C for 24 h to assure full hydration of the membrane for humidified gas measurements. The Fumasep FAAM-PK-75 membrane was put in 7 M KOH solution for 24 h, according to the manufacturer instructions, and then rinsed with deionized water before assembly. The two remaining polymer films (polyethylene [PE] 40 µm from Reichelt Chemietechnik and polytetrafluoroethylene [PTFE] 100 µm from Bola) were cleaned with isopropanol and water and then dried before assembly. For all the measurements under dry conditions, the samples were not hydrated/activated before assembly and were dried inside the cell assembly at 80 °C with an argon flow of 100 nmL min^{-1} for 24 h.

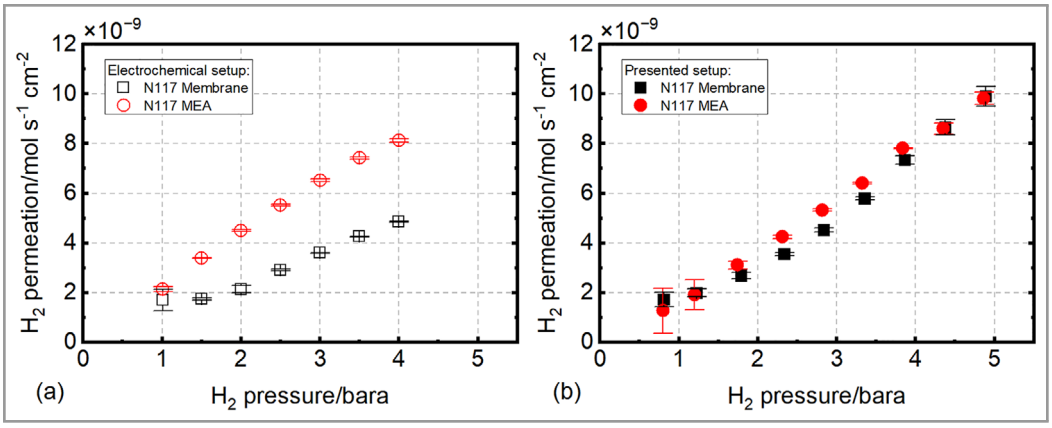

Figure 4. Comparison of hydrogen permeation obtained using (a) the electrochemical setup and (b) the setup presented in this work.

2.4 Cell Preparation

The gas crossover measurements were conducted in an in-house built electrolysis cell, with an active area of 4.4 cm by 4.4 cm (19.36 cm^2). The flow field of the anode side is made of Grade 5 titanium with platinum coating, whereas the flow field of the cathode side is coated with gold. The porous transport layer (PTL) on the anode side consists of two platinum-coated titanium fiber mats (Bekaert Currento PTL Ti-56/250 PT200) to improve mechanical support for differential pressure, whereas the PTL on the cathode side comprises of a carbon fiber mat (Toray TGP-H-60) along with a titanium gauze (Fisher Scientific Ti-Mesh 40) for mechanical support. All gaskets are made of PTFE, and the thickness was chosen to compress the carbon PTL by 50 % as per manufacturer recommendation. The cell was assembled with 8 M5 bolts that were torqued to 5 N m each crosswise.

3 Results

3.1 Comparison of Presented Setup with Electrochemical Detection Method

The primary objective of the setup presented in this study is to measure hydrogen and oxygen crossover in electrolyzer cells without necessitating disassembly, thereby preserving the integrity of the sample. Therefore, it is essential that the setup can evaluate both uncoated membranes and membranes coated with electrodes, commonly referred to as MEAs. An often utilized technique for assessing gas crossover in proton-conducting membranes is electrochemical detection [4, 25, 28]. In this method, an electrode with a defined surface area is placed in contact with the membrane, and a voltage is applied between this electrode and a counter electrode. Depending on the polarity of the applied voltage, the permeating gas is either oxidized or reduced. The resultant current is then used to calculate the molar quantity of gas diffusing through the membrane, utilizing Faraday's law.

First, a comparative analysis between the electrochemical setup described in the literature and the one introduced in this work is discussed. Fig. 4 illustrates the gas permeation results obtained using both setups ((a) hollow symbols for the electrochemical setup and (b) solid symbols for the setup introduced in this study). Both a pristine N117 membrane and an N117-based MEA were analyzed. Electrochemical measurements revealed a significant difference in gas permeation between the uncoated membrane and the MEA. This discrepancy may be attributed to the catalyst coating process, which includes hot pressing the electrode onto the membrane, potentially altering its properties. Additionally, the electrode layers introduce several microns of added thickness, which the gas must permeate. However, when applying the measurement method presented in this study, the gas permeation values of the membrane and the MEA were nearly identical, though a slight difference persisted. This residual variation may result from changes in the membrane's characteristics induced during the manufacturing process. These findings suggest that the discrepancy observed with the electrochemical setup may arise from interactions between the catalyst layer on the MEA and the catalyst-coated measurement electrode. Consequently, the presented measurement method offers a more reliable and consistent approach for evaluating and comparing gas permeation in both pristine and catalyst-coated membranes.

3.2 In Situ Measurements

To demonstrate the effectiveness of in situ measurements, an electrolysis cell featuring a Nafion N117-based MEA was assembled. The cell was initially operated for 24 h at a constant current of 1 A cm^{-2} to activate both the membrane and catalyst layer [29]. Following this activation period, the cell was directly connected to the experimental setup to assess pressure-dependent hydrogen permeation with minimal

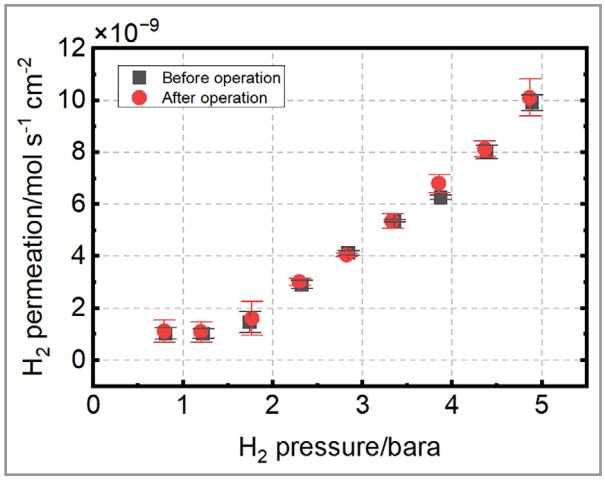

Figure 5. Pressure-dependent hydrogen permeation of an N117-based MEA before and after 7 days of operation.

modification. The electrolysis test was then resumed for an additional 7 days, after which gas permeation was re-evaluated. Fig. 5 presents the pressure-dependent permeation measurements before and after the 7-day operation, with the MEA remaining assembled in the cell throughout to avoid potential measurement artifacts caused by disassembly. In this case, due to the relatively high thickness of the N117 membrane and the short test duration, no significant increase in permeation caused by processes such as membrane thinning was observed.

3.3 Dry Versus Wet Membranes and Defect Detection

The setup also facilitates the characterization of materials in two distinct humidification states: dry and fully humidified. For instance, panel (a) of Fig. 6 illustrates a Nafion N117 membrane under both conditions. A pressure curve reflecting the permeation characteristics of both dry and wet membranes was recorded. Those data are crucial for understanding the behavior of MEAs during electrolysis at certain operating points, particularly in scenarios where effects such as excessive bubble formation can result in partial dehydration. Consequently, it offers valuable insights into the development of detailed models that describe the internal mechanisms of PEMECs and aids in analyzing the effects that occur during operation [30].

Additionally, the setup allows for the detection of mechanical defects in MEAs of PEMECs, such as pinholes. Panel (b) of Fig. 6 demonstrates the effect of a pinhole in an N115-based MEA on the total hydrogen crossover through the membrane. Under ambient or equal cathode pressure conditions, no significant difference in crossover was observed between the pristine and damaged MEAs. However, as the cathode pressure is increased, a pronounced rise in crossover is noted for the damaged sample, whereas the pristine MEA exhibits only a modest increase. Fig. 7 presents an image of the 400 µm pinhole in the damaged MEA, captured using a laser scanning microscope. This setup enables the safe testing of PEMECs for pinholes prior to operation, as it allows for the detection of hydrogen or oxygen gas crossover utilizing an inert carrier gas.

3.4 Non-PEM Membranes

The presented setup not only enables the characterization of PEMEC ionomer materials but also facilitates the evaluation of intrinsic material properties, such as hydrogen and oxygen permeability. Panel (a) of Fig. 8 presents the hydrogen permeability characteristics, whereas panel (b) shows the oxygen permeability for various polymers, including PE and PTFE, in comparison to a dry Nafion N117 membrane. These measurements are crucial for assessing the gas-tightness of materials used in gaskets and tubing within PEMECs, as well as in the associated balance-of-plant components.

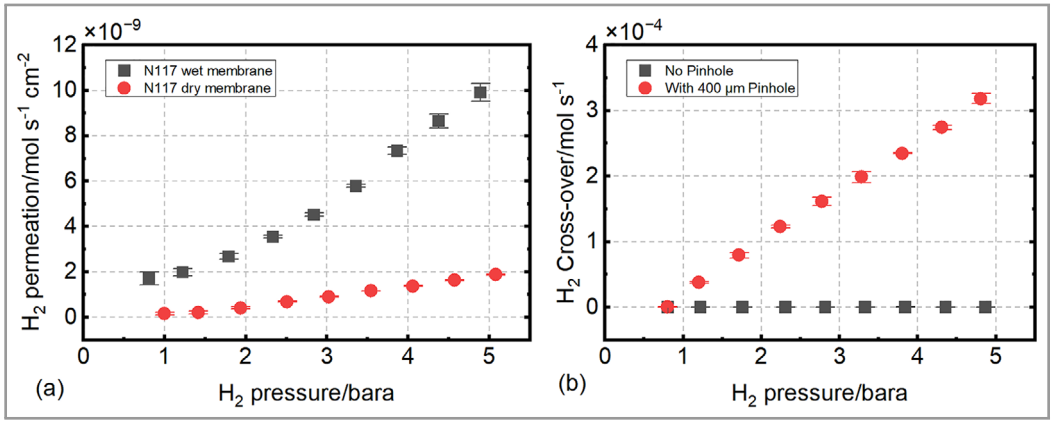

Figure 6. (a) Comparison of pressure-dependent hydrogen permeation on a wet (black) and dry (red) Nafion N117 membrane; (b) detection of a pinhole using the presented setup, via increased gas crossover.

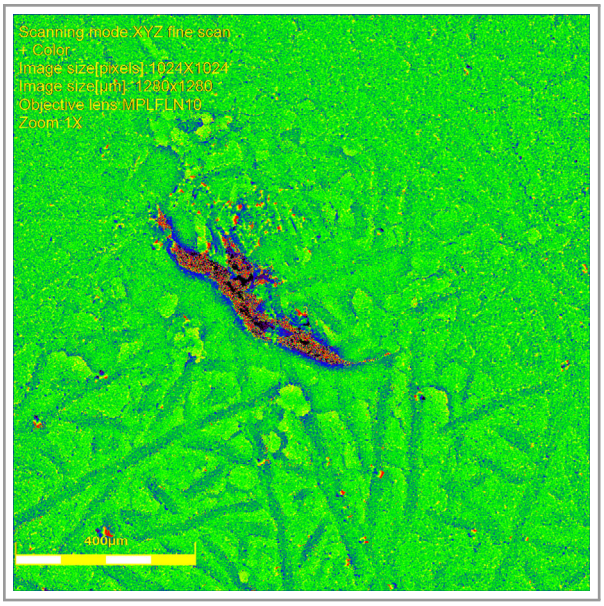

Figure 7. The image of the 400 µm pinhole, captured using a laser scanning microscope, shows distinct features. The green area represents the electrode surface, whereas the blue area highlights the edges of the crack in the membrane. The black regions indicate areas where no material was detected.

Furthermore, the setup is capable of characterizing ionomer membranes utilized in anion exchange membrane electrolysis cells (AEMECs). Panel (c) of Fig. 8 illustrates pressure-dependent permeation measurements of hydrogen, and panel (d) shows the corresponding oxygen permeation for Fumasep FAAM-PK-75 anion exchange membranes. The membrane exhibits behavior similar to that of Nafion, where increased hydration enhances gas permeation. Compared to N117, the permeation rates are higher in both dry and wet states, primarily due to the membrane's overall thinner structure.

4 Summary

A specialized setup was developed for use with PEMECs and AEMECs, enabling the measurement of hydrogen and oxygen permeation and permeability in both dry and fully humidified states. This setup allows for the direct use of electrolyzer cells, facilitating in situ membrane measurements without the need for disassembly, thereby minimizing the risk of sample alteration during testing. Additionally, it provides a pre-experiment safety check to detect pinholes in PEMECs or AEMECs prior to operation. Different types of samples and various kinds of measurements have demonstrated the broad capabilities of this setup, highlighting its versatility and wide range of potential applications.

Acknowledgments

The authors gratefully acknowledge the financial support by the German Federal Ministry of Education and Research (BMBF) within the H2Giga project DERIEL (grant number 03HY122C).

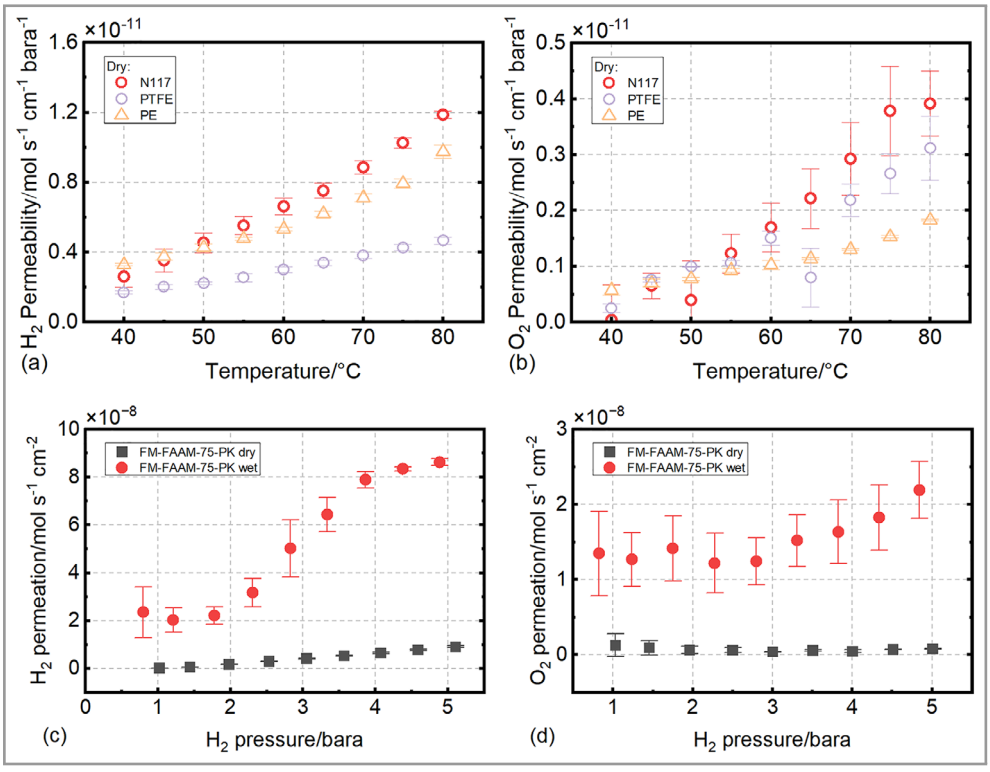

Figure 8. Temperature-dependent (a) hydrogen and (b) oxygen permeabilities of different polymers in comparison with dry Nafion N117 over varying temperatures. In (c) the hydrogen and (d) the oxygen permeation of wet and dry FM-FAAM-75-PK AEM membrane are compared.

Open access funding enabled and organized by Projekt DEAL.

Symbols used

A	[cm^{-2}]	cell area
e_{H_2}	[mol $s^{-1}cm^{-2}$]	hydrogen permeation
L	[cm]	membrane thickness
$\dot{n}_{H_2}$	[mol s^{-1}]	hydrogen crossover flow
P_{ac}	[bara]	gas pressure at actual conditions
P_n	[bara]	gas pressure at normal conditions
p_{H_2}	[bara]	partial pressure of hydrogen
p_{H_2O}	[bara]	partial pressure of water vapor
R	[J $mol^{-1}K^{-1}$]	gas constant
$X_{H_2/Ar}$	[ppm]	amount of hydrogen in argon
T_{ac}	[K]	gas temperature at actual conditions
T_{cell}	[K]	temperature of the measurement cell
T_n	[K]	gas temperature at normal conditions
$\dot{V}_{Ar,ac}$	[L s^{-1}]	volume flow of argon at actual conditions
$\dot{V}_{H_2}$	[L s^{-1}]	volume flow of hydrogen at actual conditions

Greek Letter

ε_{H_2}	[mol $s^{-1}cm^{-1}bara^{-1}$]	hydrogen permeability

References

[1] A. Karl, E. Jodat, H. Kungl, L. Dobrenizki, G. Schmid, P. Geskes, R.-A. Eichel, *Electrochem. Sci. Adv.* **2025**, *5*, e202400041. DOI: https://doi.org/10.1002/elsa.202400041

[2] S. A. Grigoriev, V. I. Porembskiy, S. V. Korobtsev, V. N. Fateev, F. Auprêtre, P. Millet, *Int. J. Hydrog. Energy* **2011**, *36* (*3*), 2721–2728. DOI: https://doi.org/10.1016/j.ijhydene.2010.03.058

[3] P. Trinke, B. Bensmann, R. Hanke-Rauschenbach, *Int. J. Hydrog. Energy* **2017**, *42* (*21*), 14355–14366. DOI: https://doi.org/10.1016/j.ijhydene.2017.03.231

[4] M. Schalenbach, T. Hoefner, P. Paciok, M. Carmo, W. Lueke, D. Stolten, *J. Phys. Chem. C* **2015**, *119* (*45*), 25145–25155. DOI: https://doi.org/10.1021/acs.jpcc.5b04155

[5] A. Martin, P. Trinke, M. Stähler, A. Stähler, F. Scheepers, B. Bensmann, M. Carmo, W. Lehnert, R. Hanke-Rauschenbach, *J. Electrochem. Soc.* **2022**, *169* (*1*), 14502. DOI: https://doi.org/10.1149/1945-7111/ac4459

[6] M. Stähler, A. Stähler, F. Scheepers, M. Carmo, W. Lehnert, D. Stolten, *Int. J. Hydrog. Energy* **2020**, *45* (*7*), 4008–4014. DOI: https://doi.org/10.1016/j.ijhydene.2019.12.016

[7] S. Fahr, F. K. Engel, S. Rehfeldt, A. Peschel, H. Klein, *Int. J. Hydrog. Energy* **2024**, *68*, 705–721. DOI: https://doi.org/10.1016/j.ijhydene.2024.04.248

[8] *PEM Electrolysis for Hydrogen Production: Principles and Applications* (Eds: D.G. Bessarabov, H. H. Wang, H. Li, N. Zhao), CRC Press, Boca Raton, London, New York **2016**.

[9] S. A. Grigoriev, P. Millet, S. V. Korobtsev, V. I. Porembskiy, M. Pepic, C. Etievant, C. Puyenchet, V. N. Fateev, *Int. J. Hydrog. Energy* **2009**, *34* (*14*), 5986–5991. DOI: https://doi.org/10.1016/j.ijhydene.2009.01.047

[10] Q. Feng, X. Yuan, G. Liu, B. Wei, Z. Zhang, H. Li, H. Wang, *J. Power Sources* **2017**, *366*, 33–55. DOI: https://doi.org/10.1016/j.jpowsour.2017.09.006

[11] H. Liu, F. D. Coms, J. Zhang, H. A. Gasteiger, A. B. LaConti, in *Polymer Electrolyte Fuel Cell Durability* (Eds: F. N. Büchi, M. Inaba, T. J. Schmidt), Springer, New York, NY **2009**.

[12] P. Frühwirt, A. Kregar, J. T. Törring, T. Katrašnik, G. Gescheidt, *Phys. Chem. Chem. Phys.* **2020**, *22* (*10*), 5647–5666. DOI: https://doi.org/10.1039/C9CP04986J

[13] *PEM Water Electrolysis Hydrogen Energy and Fuel Cells Primers* (Eds: D. Bessarabov, P. Millet), Academic Press, Cambridge USA **2018**.

[14] N. K. Moehring, A. B. Mansoor Basha, P. Chaturvedi, T. Knight, X. Fan, P. N. Pintauro, M. S. H. Boutilier, K. Karan, P. R. Kidambi, *Nano Lett.* **2025**, *25* (*3*), 1165–1176. DOI: https://doi.org/10.1021/acs.nanolett.4c05725

[15] Y. Nagao, *ChemElectroChem* **2024**, *11* (*12*), e202300846. DOI: https://doi.org/10.1002/celc.202300846

[16] S. Siracusano, S. Trocino, N. Briguglio, V. Baglio, A. S. Aricò, *Materials* **2018**, *11* (*8*), 1368. DOI: https://doi.org/10.3390/ma11081368.

[17] A. Martin, P. Trinke, B. Bensmann, R. Hanke-Rauschenbach, *J. Electrochem. Soc.* **2022**, *169* (*9*), 94507. DOI: https://doi.org/10.1149/1945-7111/ac908c

[18] A. Martin, P. Trinke, M. Stähler, A. Stähler, F. Scheepers, B. Bensmann, M. Carmo, W. Lehnert, R. Hanke-Rauschenbach, *J. Electrochem. Soc.* **2022**, *169* (*1*), 14502. DOI: https://doi.org/10.1149/1945-7111/ac4459

[19] M. Schalenbach, M. Carmo, D. L. Fritz, J. Mergel, D. Stolten, *Int. J. Hydrog. Energy* **2013**, *38* (*35*), 14921–14933. DOI: https://doi.org/10.1016/j.ijhydene.2013.09.013

[20] A. Stähler, M. Stähler, F. Scheepers, W. Lehnert, M. Carmo, *J. Electrochem. Soc.* **2022**, *169* (*3*), 34522. DOI: https://doi.org/10.1149/1945-7111/ac5c9b

[21] P. Trinke, G. P. Keeley, M. Carmo, B. Bensmann, R. Hanke-Rauschenbach, *J. Electrochem. Soc.* **2019**, *166* (*8*), F465. DOI: https://doi.org/10.1149/2.0171908jes

[22] P. Trinke, B. Bensmann, R. Hanke-Rauschenbach, *Electrochem. Commun.* **2017**, *82*, 98–102. DOI: https://doi.org/10.1016/j.elecom.2017.07.018

[23] M. Bernt, J. Schröter, M. Möckl, H. A. Gasteiger, *J. Electrochem. Soc.* **2020**, *167* (*12*), 124502. DOI: https://doi.org/10.1149/1945-7111/abaa68

[24] A. Parthasarathy, S. Srinivasan, A. J. Appleby, C. R. Martin, *J. Electrochem. Soc.* **1992**, *139* (*9*), 2530. DOI: https://doi.org/10.1149/1.2221258

[25] V. A. Sethuraman, S. Khan, J. S. Jur, A. T. Haug, J. W. Weidner, *Electrochim. Acta* **2009**, *54* (*27*), 6850–6860. DOI: https://doi.org/10.1016/j.electacta.2009.06.068

[26] Z. Ogumi, Z. Takehara, S. Yoshizawa, *J. Electrochem. Soc.* **1984**, *131* (*4*), 769. DOI: https://doi.org/10.1149/1.2115696

[27] U.S. Department of Commerce, *Water*, U.S. Department of Commerce, Washington, DC **2023**, https://webbook.nist.gov/cgi/cbook.cgi?ID=C7732185&Mask=45&ype=ANTOINE5&Plot=on

[28] M. A. V. Devanathan, Z. Stachurski, F. C. Tompkins, *Proc. R. Soc. Lond. A, Math. Phys. Sci.* **1997**, *270* (*1340*), 90–102. DOI: https://doi.org/10.1098/rspa.1962.0205

[29] N. Wolf, A. Javed, L. Treutlein, H. Kungl, A. Karl, E. Jodat, R.-A. Eichel, *Electrochem. Sci. Adv.* **2025**, *5*, e202400038. DOI: https://doi.org/10.1002/elsa.202400038

[30] V. Karyofylli, Y. Danner, K. Ashoke Raman, H. Kungl, A. Karl, E. Jodat, R.-A. Eichel, *J. Power Sources* **2024**, *600*, 234209. DOI: https://doi.org/10.1016/j.jpowsour.2024.234209

